J. Fluid Mech. (1991), *vol.* 224, *pp.* 1–27
Printed in Great Britain

On the refraction of shock waves at a slow–fast gas interface

By L. F. HENDERSON†, P. COLELLA‡ AND E. G. PUCKETT¶
Lawrence Livermore National Laboratory, Livermore, CA 94550, USA

(Received 24 November 1989 and in revised form 12 June 1990)

We present the results of numerical computations of the refraction of a plane shock wave at a CO_2/CH_4 gas interface. The numerical method was an operator split version of a second-order Godunov method, with adaptive grid refinement. We solved the unsteady, two-dimensional, compressible, Euler equations numerically, assuming perfect gas equations of state, and compared our results with the experiments of Abd-El-Fattah & Henderson. Good agreement was usually obtained, especially when the contamination of the CH_4 by the CO_2 was taken into account. Remaining discrepancies were ascribed to the uncertainties in measuring certain wave angles, due to sharp curvature, poor definition, or short length of the waves at large angles of incidence. All the main features of the regular and irregular refractions were resolved numerically for shock strengths that were weak, intermediate, or strong. These include free precursor shock waves in the intermediate and strong cases, evanescent (smeared out) compressions in the weak case, and the appearance of an extra expansion wave in the bound precursor refraction (BPR). The structure of a BPR was elucidated for the first time.

1. Introduction

We consider two gases meeting along a plane interface, and we assume for simplicity that they both obey the perfect gas equation of state (figure 1). We suppose that a plane incident shock i of wave velocity U_i is propagated into one of the gases by the impulsive motion of a rigid boundary, such as a piston which drives into the gas at a velocity U_{pi} with $|U_{pi}| < |U_i|$. We also assume that all the boundaries of the system are adiabatic. Subsequently i meets the interface between the gases at an angle of incidence $\alpha_i = 0$ measured with respect to the interface. The shock i now begins to pass from the first, or incident gas I, into the second, or receiving gas II, where it becomes the transmitted shock t. When its new velocity U_t differs in magnitude from U_i, then by definition i has been refracted. Formally the relative refractive index n is defined by (Henderson 1989)

$$n \equiv \frac{|U_i|}{|U_t|}. \tag{1.1}$$

† Permanent address: The Institute of Space and Astronautical Science, 3-1-1 Yoshinodai, Sagamihara, Kanagawa, 229, Japan.
‡ Permanent address: Department of Mechanical Engineering, University of California, Berkeley, CA 94720, USA.
¶ Permanent address: Department of Mathematics, University of California, Davis, CA 95615, USA.

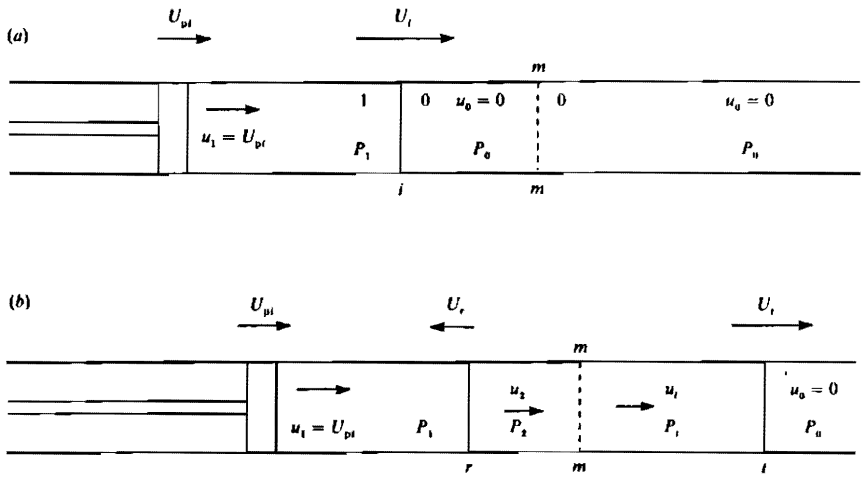

FIGURE 1. Refraction of a normal shock wave i at zero angle of incidence, $\alpha_i = 0$, at a plain interface between two media: (*a*) before refraction; (*b*) after refraction.

The refraction is slow–fast when $n < 1$; fast–slow when $n > 1$; and there is no refraction when $n = 1$.

If in laboratory frame the velocities of the gas upstream and downstream of the incident shock are u_0 and u_1 respectively, then the piston velocity is

$$U_{pi} = u_i - u_0.$$

In this frame of reference the gas upstream of i is undisturbed, so that $u_0 = 0$, and the boundary condition then becomes simply, $U_{pi} = u_1$.

In general a reflected wave is also produced at the gas interface by the refraction (figure 1*b*). When i is a shock then so also will be t, but the reflected wave may be either an expansion e, or a shock r. It is assumed that there is always continuity in the pressure P and in the particle velocity u across the interface. Following refraction this gives

$$P_2 = P_t, \tag{1.2}$$

$$u_2 = u_t. \tag{1.3}$$

The nature of the reflected wave may be determined with the help of (1.2) and (1.3) together with the notion of wave impedance Z. For head-on refraction at angle of incidence $\alpha_i = 0$ the incident wave impedance, Z_i, is defined by

$$Z_i \equiv \frac{P_1 - P_0}{u_1 - u_0} = \frac{P_1 - P_0}{U_{pi}}.$$

Alternatively, in shock wave coordinates we have

$$Z_i = -\frac{u_0}{v_0} = -\rho_0 u_0 = \rho_0 U_i, \tag{1.4}$$

$$Z_i = -\frac{u_1}{v_1} = -\rho_1 u_1, \tag{1.5}$$

where ρ is the density, v is the specific volume, and we have used the fact that in shock wave coordinates $u_0 = -U_i$. (In general, an upper case U (U_i, U_{pi}, etc.) always denotes a velocity with respect to laboratory coordinates whereas a small case u (u_0, u_1, etc.) may denote a velocity in laboratory coordinates or shock wave coordinates depending on the context.) The transmitted and reflected wave impedances Z_t and Z_r are defined similarly. The pressure reflection (R) and transmission (T) coefficients are

$$R \equiv \frac{P_2 - P_1}{P_1 - P_0} = \frac{Z_r}{Z_i}\frac{Z_t - Z_i}{Z_t - Z_r}, \tag{1.6}$$

$$T \equiv \frac{P_t - P_0}{P_1 - P_0} = \frac{Z_t}{Z_i}\frac{Z_t - Z_r}{Z_t - Z_r}, \tag{1.7}$$

with similar expressions for the shock intensity which is the average power flux through unit area in the direction of propagation, and the coefficient for the total power transmitted (Henderson 1989). The coefficients (1.6) and (1.7) show that when the impedance increases during refraction $|Z_t| > |Z_i|$, then a shock r will be reflected from the interface back into the incident gas because then $R > 0$, but that when it decreases $|Z_t| < |Z_i|$, then we obtain a reflected expansion with $R < 0$. When the impedances are equal, $Z_t = Z_i$, there is no reflected wave even though the two gases may differ in composition or in states. In this case $R = 0$. Now combining (1.4) for Z_i and Z_t with (1.1) we obtain

$$n = \frac{|U_i|}{|U_t|} = \frac{v_0 Z_i}{v_t Z_t}, \tag{1.8}$$

where v_t is the specific volume of the gas upstream of the t shock. So even with $Z_i = Z_t$, the wave will still be refracted if $v_t \neq v_0$.

More generally, the incident shock may meet the gas interface at a non-zero angle of incidence $\alpha_i \neq 0$ (figure 2*a*), and different refraction phenomena then occur. The wave systems illustrated in figure 2(*a–c*) are called *regular refractions* by analogy with von Neumann's (1943) classification of regular and Mach *reflections*. His theory of regular reflection is easily extended to regular refraction and the results are in good agreement with experiment (Jahn 1956; Abd-El-Fattah, Henderson & Lozzi 1976; Abd-El-Fattah & Henderson 1978*a*, *b*).

If a regular wave system is to exist, then all of its waves must travel at the same velocity U along the interface, and this fact gives immediately the *fundamental law of refraction*, namely

$$|U| = \frac{|U_i|}{\sin\alpha_i} = \frac{|U_t|}{\sin\alpha_t} = \frac{|U_r|}{\sin\alpha_r} = \frac{|U_j|}{\sin\alpha_j}, \tag{1.9}$$

where U_j is the velocity of any wave in the reflected and centred expansion wave, and α_j is the corresponding wave angle (figure 2*c*). Evidently, $|U_j| = c_j$, which is the local speed of sound. Under certain conditions this law may be violated; for example with a continuous increase in the parameter α_i the regular wave system may break up with the t shock moving ahead of the incident and reflected waves to form some type of irregular refraction with precursor waves (figure 2*d–f*). In this event,

$$\frac{|U_i|}{\sin\alpha_i} > \frac{|U_t|}{\sin\alpha_t} = \frac{|U_r|}{\sin\alpha_r} = \frac{|U_j|}{\sin\alpha_j}. \tag{1.10}$$

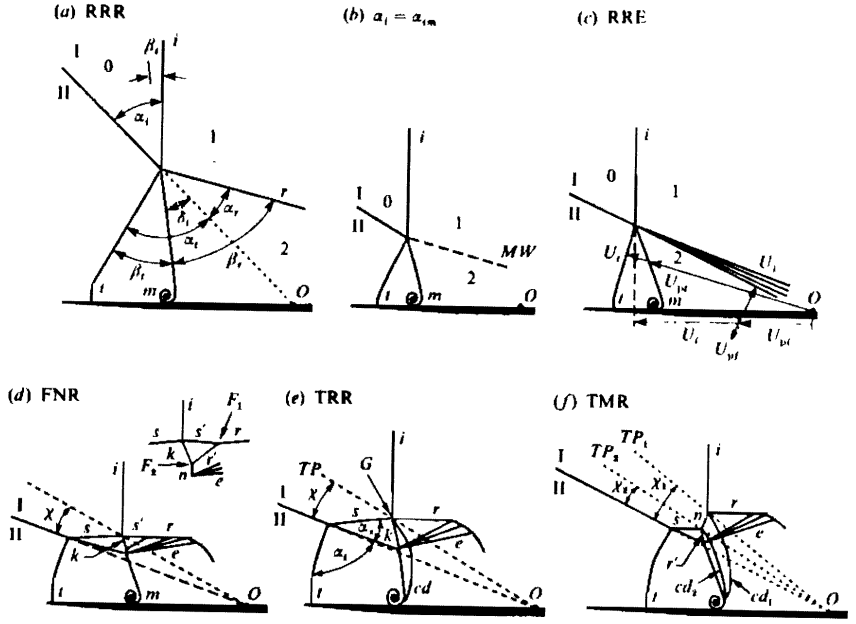

FIGURE 2. (*a–e*) Regular and (*d–f*) irregular shock refraction systems for a slow–fast CO_2/CH_4 gas interface, $n < 1$. (*a*) Reflected shock, RRR, $|Z_r| > |Z_i|$, $\alpha_t > \alpha_i$; (*b*) reflected Mach line degeneracy, $|Z_r| = |Z_i|$, $\alpha_t > \alpha_i = \alpha_{im}$; (*c*) reflected expansion, RRE, $|Z_r| < |Z_i|$, $\alpha_t > \alpha_i$; (*d*) free precursor von Neumann refraction, FNR; (*e*) twin regular reflection–refraction, TRR; (*f*) twin Mach reflection–refraction, TMR. *i*, Incident shock; *t*, transmitted shock; *r*, *r'*, reflected shocks; *e*, reflected expansion wave; *k*, modified incident shock; *n* Mach shock; *s*, side shock; *s'*, modified side shock, *m* gas interface; I, Region of undisturbed CO_2; II, region of undisturbed CH_4; *MW*, Mach line; $cd_{(1,2)}$, contact discontinuity; $TP_{(1,2)}$, trajectory path of shock wave confluences; $\chi_{(1,2)}$, trajectory path angles of shock wave confluences; $F_{1,2}$, shock triple points; *G*, quadruple point; *O* origin where *i* first encountered gas interface.

For oblique refraction, $\alpha_t > 0$, it is necessary to generalize the definition of wave impedance to

$$Z_t \equiv \frac{P_t - P_0}{U_{pt}\cos\beta_t},$$

where β_t is the wave angle measured with respect to the *disturbed* gas interface (figure 2*a*). Similar expressions are defined for the other waves, and with these definitions (1.6) and (1.7) remain valid.

The refraction law (1.9) may be combined with the definitions of n, Z_i, and Z_t to extend (1.8) to

$$n = \frac{|U_t|}{|U_i|} = \frac{\sin\alpha_t}{\sin\alpha_i} = \frac{\nu_0 Z_t \cos\beta_t}{\nu_i Z_i \cos\beta_i}. \tag{1.11}$$

The particular angle α_i for which there is equality of impedance, $Z_t = Z_i$, is called the *angle of intromission* $\alpha_i = \alpha_{im}$, as in acoustic theory. The wave i is still refracted at this condition because in general $n \neq 1$ when $\alpha_i = \alpha_{im}$ (figure 2*b*).

Using the refraction law we may also write

$$\cos\alpha_t = (1-\sin^2\alpha_t)^{\frac{1}{2}} = (1-n^{-2}\sin^2\alpha_i)^{\frac{1}{2}}.$$

Thus $\cos\alpha_t$ becomes pure imaginary when $1-n^{-2}\sin^2\alpha_i < 0$, that is when α_i exceeds the *normal critical angle*, α_c, which is defined by

$$\sin\alpha_c = n = \frac{|U_t|}{|U_i|}. \tag{1.12}$$

Clearly α_c only exists for slow–fast refraction, $n < 1$. At the critical condition, t is perpendicular to the gas interface $\alpha_t = \frac{1}{2}\pi$; that is, it is a normal shock. Accordingly the gas interface is not deflected in this special case and it remains everywhere in a single plane. It follows that when the pressure P_2 is applied to the receiving gas it causes no deflection of the interface, so that it behaves like a rigid surface. In this sense $|Z_t| = \infty$, when $\alpha_i = \alpha_c$. In summary, by (1.11) n is a measure of the capacity of the gases to bend or refract the incident shock, while by (1.6) and (1.7) the wave impedances determine the nature of the reflected and transmitted waves.

Whitham's (1958, 1959) theory has been extended in an attempt to describe both regular and irregular refractions (Catherasoo & Sturtevant 1983; Schwendeman 1988). It is attractive not only for its simplicity but also because it often agrees remarkably well with experiment. However, it is an approximate theory, and it does not describe wave reflections properly, nor disturbances that arise in the downstream flow and subsequently overtake a shock. In refracting systems difficulties can also arise which are apparently associated with the formation of a 'shock shock' on an interface, or even when one is close to it. Furthermore it cannot deal with shock discontinuities at a gas interface (Catherasoo & Sturtevant 1983).

By contrast the von Neumann theory is exact (within its assumptions) but it is only adequate for describing regions of uniform flow, which restricts it to regular refractions. Irregular refractions have non-uniformities and it is then necessary to solve the equations of motion everywhere in order to obtain an adequate description of the phenomena.

In the present paper, we present the results of our numerical studies of slow–fast refraction with particular emphasis on the irregular systems. The numerical method that we used is an adaption of second-order, finite-difference solution of the Euler and continuity equations for the two-dimensional, unsteady, compressible flow of perfect gases. It is an operator split version of the second-order Godunov method developed by van Leer (1979), Collela & Glaz (1985), and Colella & Woodward (1984). The results are compared with the experimental data of Abd-El-Fattah & Henderson (1978*b*). Agreement with experiment is satisfactory for much of the data, particularly if allowance is made for the effects of gas contamination in the experiment. Some discrepancies do exist, especially for the α_t data for irregular systems. This is ascribed to uncertainties in the measurements caused by the sharp curvature of the transmitted wave at large angles of incident α_i.

2. The experiments

The experimental method has been described by Bitondo (1950), Jahn (1956), Abd-El-Fattah *et al.* (1976), and Abd-El-Fattah & Henderson (1978*a*, *b*). The experiments of the last named authors appear to be the most extensive and we describe them briefly. A delicate polymer membrane was set up in a shock tube; its functions were to define the initial gas interface as a plane surface, and to prevent the gases from mixing until the incident shock arrived. The mass of the membrane was between 0.5 and 1.0×10^{-4} kg m^{-2}, and its thickness was between 5.5 and 6.5×10^{-6} m.

In order to set up a slow–fast interface such as CO_2/CH_4, the CO_2 was slowly introduced onto one side of the membrane while the CH_4 was introduced onto the other. The gases were continuously circulated through the shock tube to minimize mutual contamination by diffusion and leakage across the membrane. The contamination was monitored continuously by a thermal conductivity meter, and typically the CH_4 was contaminated by about 10% by volume with CO_2, but the CO_2 was much purer. It should be noted that the volume of CO_2 in the shock tube was about 250 times larger than the CH_4.

A shock of prescribed inverse strength $\xi_i \equiv P_0/P_1$, was started in the CO_2, and arranged to strike the membrane/gas interface at a predetermined angle of incidence α_i. The shock shattered the membrane and entered the CH_4, and was thus refracted. The wave system was photographed by a schlieren optical system, and transducers measured the speed and strength of the incident shock.

Recently, Haas & Sturtevant (1987) have experimented with weak shocks refracting at cylindrical and spherical interfaces. The gases were initially prevented from mixing by the use of plastic membranes or soap bubbles. However, in the interest of simplicity we will confine our attention to plane gas interfaces.

3. The computations

3.1. *The numerical method*

We used a second-order finite-difference solution of the Euler and continuity equations on a rectangular grid with reflecting boundary conditions on three sides and inflow boundary conditions on the fourth. The numerical integration of the equations was accomplished with an operator split version of a second-order Godunov method (van Leer 1979; Colella & Woodward 1984). In our implementation we employed the efficient algorithm for the solution of the Riemann problem developed by Colella & Glaz (1985). Since the method is a conservative finite-difference scheme, mass, momentum, and energy were all conserved. The method is accurate to second order in space and time for smooth flow, and captures shocks and other discontinuities with minimum numerical overshoot and dissipation. It has been used quite extensively to compute unsteady shock reflections in gases, and has a demonstrated ability to resolve complex interactions of discontinuities in good agreement with experiment (Glaz *et al.* 1985).

An important feature of the numerical method is that it employs a dynamic regridding strategy called adaptive mesh refinement (AMR). This entails placing a finer, rectangular grid over any region of particular interest or excessive error, with the grid spacing being reduced by an even factor – typically 2 or 4. The boundary of the refined grid always coincided with the cell edges of the coarse grid. Multiple levels of refinement were possible with the maximum number of nested grids being supplied as a parameter by the user. In the present work, we determined those regions that required refinement by estimating the local truncation error in the density, and refining wherever the error was greater than an initially specified amount. In addition, we refined to the maximum extent all multifluid cells (those containing both gases) and all cells lying within two cell widths of a multifluid cell. Special care was taken to ensure that the fluxes on boundaries between coarse and fine grids matched; the details are given by Berger & Colella (1989). Adaptive gridding was a crucial component of our method which enabled us to resolve important features of the flow economically. A typical run with two levels of gridding and a refinement factor of 4 took 10 minutes of CPU time on a CRAY XMP computer.

	Pure carbon dioxide	Pure methane	Contaminated methane
γ	1.288	1.303	1.301
μ	44.01	16.04	18.84

TABLE 1. Properties of the pure and contaminated gases

The gas interface was modelled using an algorithm of Noh & Woodward (1976) known as SLIC (Simple Line Interface Calculation). Here a number f_{ij}, between 0 and 1, and called the volume fraction, was associated with each grid cell through which the gas interface passed. This f_{ij} was the volume fraction of the cell occupied by one of the gases. Obviously the other gas occupied the fraction $1-f_{ij}$. During each integration sweep a simple picture of the interface consisting entirely of vertical and horizontal line segments was constructed from this volume fraction information. This was used to determine how much of each gas was convected out of the cell and into adjacent cells on this pass, and hence to update the volume fractions associated with each cell. One of the drawbacks of volume-of-fluid-based interface tracking schemes such as SLIC is that in a region undergoing expansion or compression both of the gases in a multifluid cell will be expanded or compressed equally, in spite of the density differences that may exist between them. To use this method with the present problem we incorporated a scheme due to Colella, Ferguson & Glaz (1990) in which the equations of gas dynamics are supplemented with evolution equations for the volume fraction, total energy, and mass density of each gas in the multifluid cells. This formulation takes into account the compressibility of each gas component in a multifluid cell so as to ensure the correct individual expansions or compressions.

3.2. *Outline and plan of the numerical work*

We shall present the results of our computations as though we had done a series of experiments in a shock tube. This means that in a particular sequence, the ratios of the specific heats γ_t, γ_i of the gases and their molecular weights μ_t, μ_i were held constant and so also was ξ_i. The only parameter that varied through the sequence was α_i. This was assumed to be initially near the condition for head-one incidence at $\alpha_i = 0$; it was then increased in discrete steps until it approached glancing incidence at $\alpha_i = \frac{1}{2}\pi$; thus $0 < \alpha_i < \frac{1}{2}\pi$. A particular refraction was uniquely defined once the values of $(\gamma_t, \gamma_i, \mu_t, \mu_i, \xi_i, \alpha_i)$ together with the system boundaries were given. Typically the phenomena that appeared from this procedure were a sequence of regular refractions followed by an irregular sequence.

We shall compare our numerical results with the experimental data obtained by Abd-El-Fattah & Henderson (1978*b*) for the slow–fast, $n < 1$, CO_2/CH_4 gas interface. There were two artifacts in those experiments which we took into account in our computations in order to make the comparison as accurate as possible. These were the inertia of the membrane and the contamination of the gases by diffusion and leakage across it.

Membrane inertia We calculated the membrane density from the published data, and it was about 680 times denser than CO_2 at standard conditions. Using this factor in the computations, the membrane was treated as though it were superdense carbon dioxide. Generally its effect was negligible; all we noticed was a slight displacement in the pressure contours when the contours were compared with, and without, the

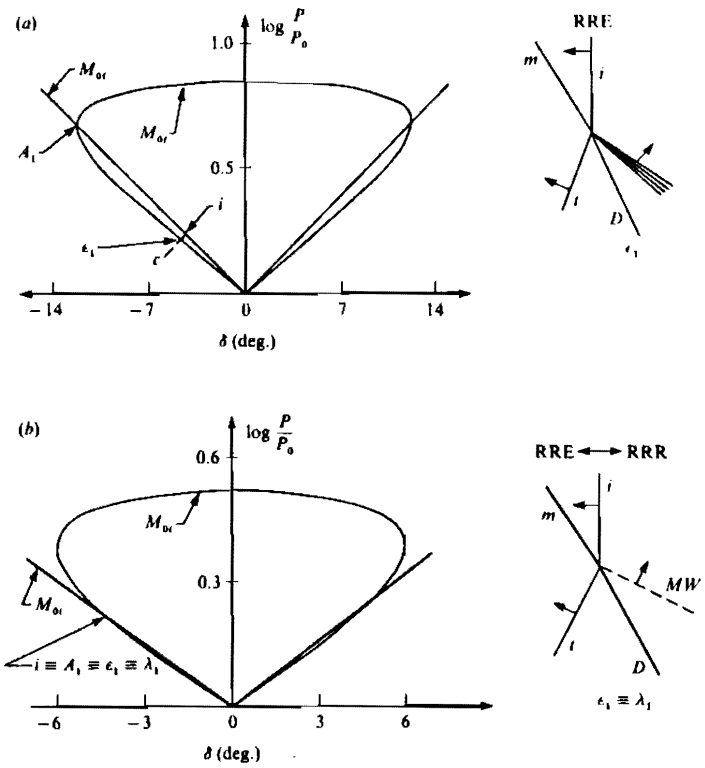

FIGURE 3(a, b). For caption see page 10.

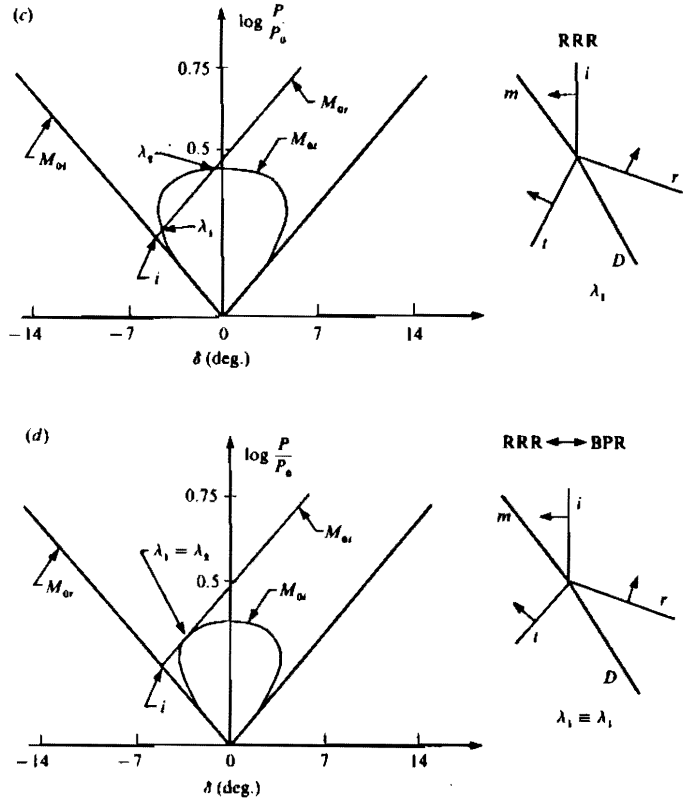

FIGURE 3(c, d). For caption see next page.

membrane for the same refractions. In view of this we deleted it from the remainder of our computations.

Gas contamination The published data showed that the methane was contaminated by about 10% by volume with carbon dioxide, but that the CO_2 itself was approximately pure. (Remember their volume ratio in the shock tube was about 250:1 in favour of the CO_2.) The properties of the pure and contaminated gases are presented in table 1. Contamination is a significant effect and it will be discussed below.

4. Results and discussion for a weak shock refraction sequence

4.1. *The polar diagrams*

The sequence and its polar diagrams are presented in figure 3. They are similar to the ones described by Abd-El-Fattah & Henderson although here we assume that the CH_4 is not contaminated by the CO_2. When α_t is comparatively small, there is a regular refraction with a reflected expansion (RRE) (figure 3*a*), so $|Z_t| < |Z_i|$, $R < 0$, $1 > T > 0$. Since the refraction is slow–fast, $n < 1$, we have by (1.11) that $\alpha_t > \alpha_i$, that is t is steeper than i. The reflection e_1 is a centred, Prandtl–Meyer, expansion fan and it is plotted in the polar diagram as the isentropic curve c. It intersects the polar for the t shock at the point ϵ_1 which defines the von Neumann solution for RRE. The solution requires there to be continuity in the pressure and in the streamline direction δ, everywhere along the gas interface. Although (1.2) remains valid when $\alpha_t \neq 0$, (1.3) must be replaced by

$$\delta_0 + \delta_1 = \delta_t, \tag{4.1}$$

where δ_0, δ_1 and δ_t are the deflection angles for the i, r and t waves respectively. This is the continuity condition for the streamline direction. It is sometimes convenient to replace (1.2) by the equivalent expression

$$(P_2 - P_1) + (P_1 - P_0) = (P_t - P_0).$$

For reflected expansions we must replace (4.1) by

$$U_{pt}\cos\beta_t + \int_1^2 \cos\beta_j \, dU_{pj} = U_{pt}\cos\beta_t,$$

where U_{pi}, U_{pt}, are the driving piston velocities of the i and t shocks, dU_{pj} is the infinitesimal withdrawing piston velocity for an arbitrary jth wave in the reflected expansion, and $\beta_i, \beta_t, \beta_j$ are the wave angles which are defined with respect to the *disturbed* gas interface (figure 2*a* and 2*c*).

If α_t is now increased continuously, the polars shrink somewhat and the

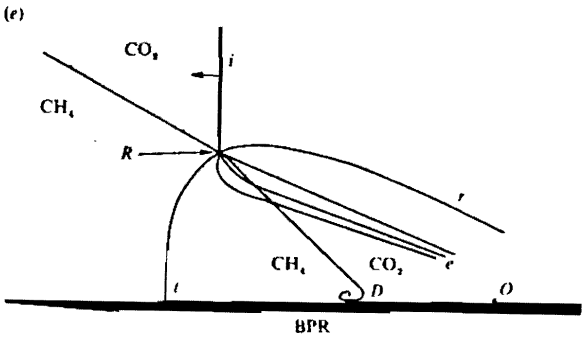

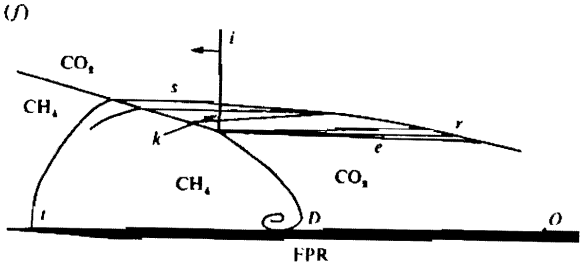

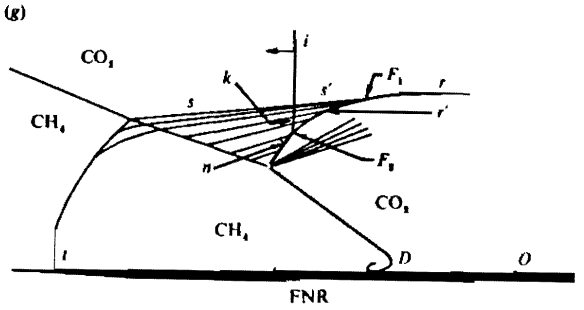

FIGURE 3. Polar diagrams for a weak shock refraction sequence with $\xi_4 = 0.78$ at a pure CO_2/CH_4 gas interface. (*a–c*) Regular refraction, (*d*) transition, and (*e–g*) irregular refraction. (*a*) Reflected expansion, RRE, at $\alpha_i = 27°$, $|Z_t| < |Z_i|$; (*b*) degenerate refraction at the angle of intromission $\alpha_i = \alpha_{im} \approx 32.0592°$, $Z_t = Z_i$, $R = 0$, $T = 1$, the condition for total energy transmission; (*c*) reflected shock, RRR, at $\alpha_i = 33.27°$, $|Z_t| > |Z_i|$; (*d*) the shock critical angle $\alpha_{sc} \approx 34.4885°$; (*e*) bound precursor refraction, BPR, $\alpha_i > \alpha_{sc}$; (*f*) free precursor refraction, FPR, *s* and *t* are evanescent waves; (*g*) free precursor von Neumann refraction, FNR, M_{0i}, M_{0t}, M_{0r}, free-stream Mach numbers upstream, and relative to the *i*, *t*, and *r* shocks respectively; $(\epsilon_1, \lambda_1, \lambda_2)$ solutions of the von Neumann regular refraction theory; *D*, disturbed gas interface; A_1, intersection point of the primary polars (i, t). For other symbols see the caption to figure 2.

intersection point A_1 of the primary polars (i, t) moves downwards towards the point i which is the map of the incident shock. As this happens the strength $|P_2 - P_1|$ of the expansion decreases and eventually vanishes at the angle of intromission $\alpha_i = \alpha_{im} \approx 32.0592°$, which corresponds to $\epsilon_1 \equiv i \equiv A_1$. The reflection is reduced to a Mach line degeneracy $|P_2 - P_1| = 0$ and the other wave impedances become equal: $Z_t = Z_i, R = 0, T = 1$. This is the condition for *total transmission*, and here also $\alpha_t > \alpha_i$ (figures 2*b*

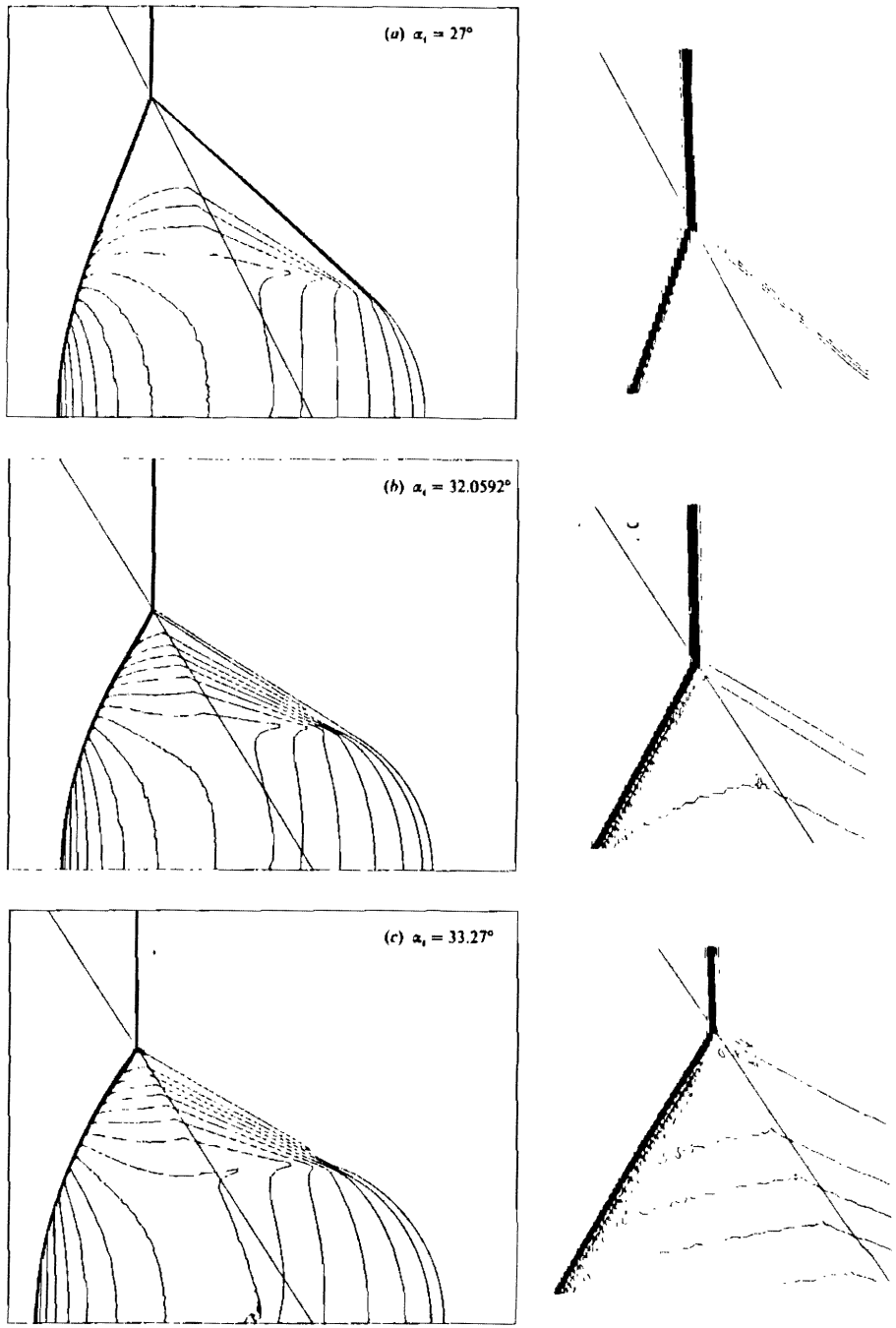

FIGURE 4(*a–c*). For caption see page 13.

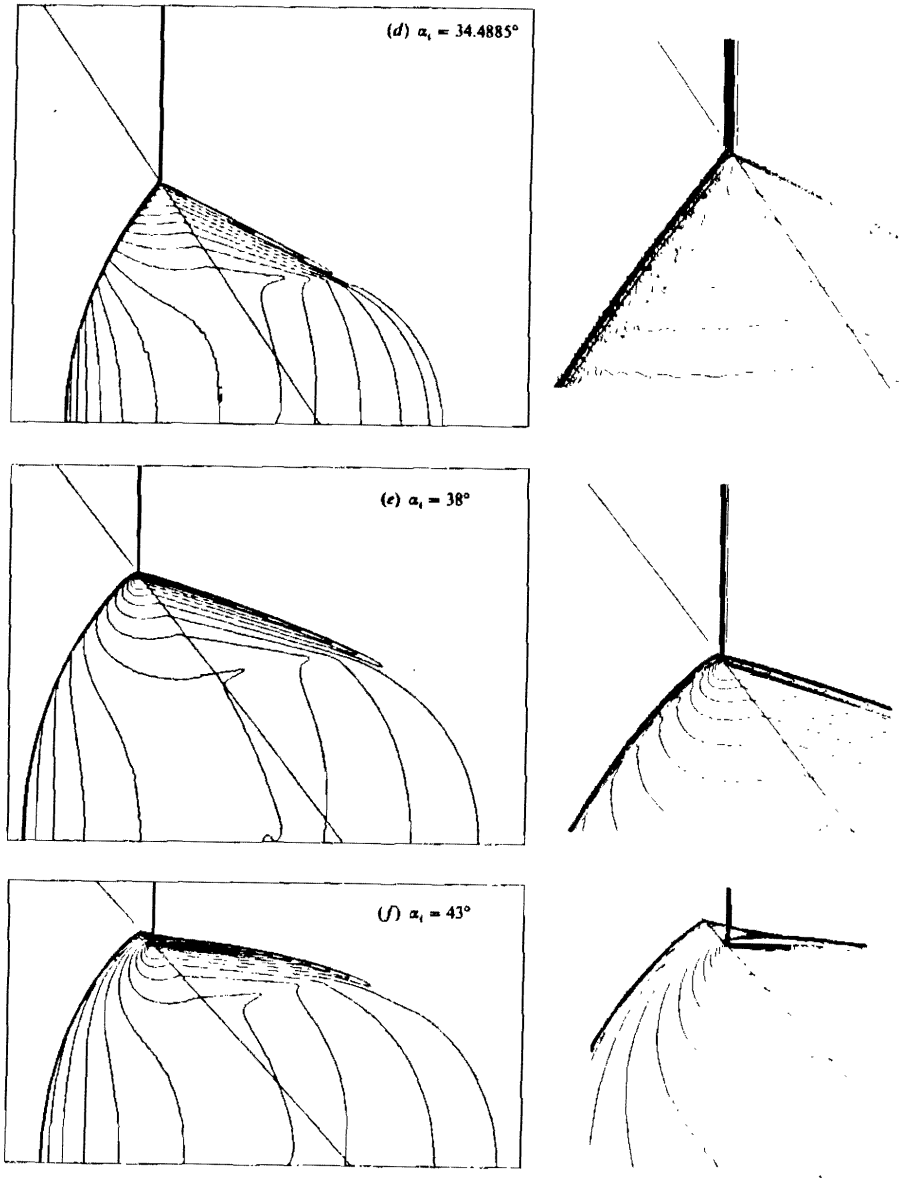

FIGURE 4(*d–f*). For caption see facing page.

and 3*b*). As α_i continues to increase, $\alpha_i > \alpha_{im}$, the reflection becomes a shock (RRR) (figure 3*c*), and now $|Z_t| > |Z_i|$, $R > 0$, $T > 1$, with again $\alpha_t > \alpha_i$. The von Neumann theory gives two solutions λ_1 and λ_2 for RRR, but experiment shows that it is the weaker λ_1 solution which appears physically. In this respect note that λ_1 is the continuation of the ϵ_1 solution while λ_2 is not; in fact at the intromission angle, ϵ_1 and λ_1 are identical and degenerate: $\epsilon_1 \equiv \lambda_1 \equiv A_1 \equiv i$.

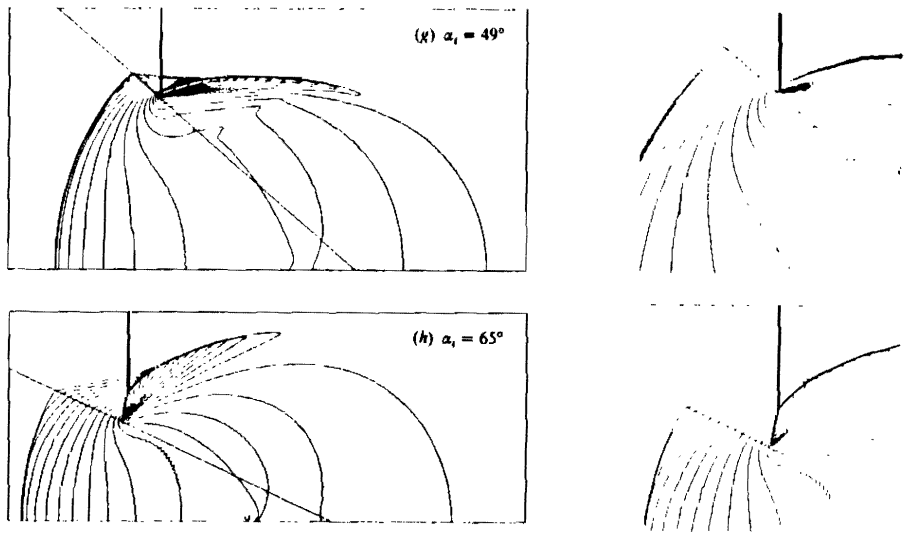

FIGURE 4. Contour plots of log P for a weak shock refraction sequence with $\xi_i = 0.78$ at a pure CO_2/CH_4 gas interface. (*a*) $\alpha_i = 27°$, RRE; (*b*) total transmission at the angle of intromission, $\alpha_i = \alpha_{im} \approx 32.0592°$; (*c*) $\alpha_i = 33.27°$, RRR; (*d*) RRR$\rightleftharpoons$BPR, $\lambda_1 \equiv \lambda_2$, at the shock critical angle $\alpha_{sc} \approx 34.4885°$; (*e*) $\alpha_i = 38°$, BPR; (*f*) $\alpha_i = 43°$, FPR; (*g*) $\alpha_i = 49°$, FPR; (*h*) $\alpha_i = 65°$, FNR. (The straight line running diagonally from upper left to lower right represents the initial, undisturbed gas interface. It is not a pressure contour.)

As α_i continues to increase, λ_1 and λ_2 approach each other and eventually coincide, $\lambda_1 = \lambda_2$ (figure 3*d*). This takes place at the *shock critical angle* $\alpha_i = \alpha_{sc} \approx 34.488°$. In general this angle does *not* coincide with the *normal critical angle* α_c, defined by (1.12), and usually occurs before it, $\alpha_{sc} < \alpha_c$. For $\alpha_i > \alpha_{sc}$, the λ_1 and λ_2 solutions are no longer physically significant because they are unreal. The refraction is now irregular and precursor compression waves may develop (figure 3*e–g*). In the experiments of both Jahn and Abd-El-Fattah & Henderson the precursors did not appear as soon as the shock critical angle was exceeded. In fact, α_i had to increase somewhat beyond α_{sc} before they were observed. We shall return to this point later.

4.2. *The numerical results for the sequence*

The numerical results presented here are all for *uncontaminated* gases with *no membrane*. We believe that these results will be of more general interest than those which include the artifacts of the experiments. Selected contour plots for the sequence are shown in figure 4, a schlieren photograph from the experiments is shown in figure 5(*a*) and colour contour plots to compare with the schlieren photograph are shown in figure 5(*b*, *c*) (plate 1). Of course the comparison can only be qualitative because the numerical results do not include the artifacts. However, note that the numerical results exhibit all of the essential features of the flow which are found in the schlieren photo and that these features appear to be in the same relation to one another as in the schlieren. We present a more detailed comparison in §4.4 below.

Incidentally, we prefer the colour contour plots to grey scale plots of the same quantities because we believe that the eye is more sensitive to changes in colour than to changes in contrast. We find that colour reveals more detail such as very weak

(a)

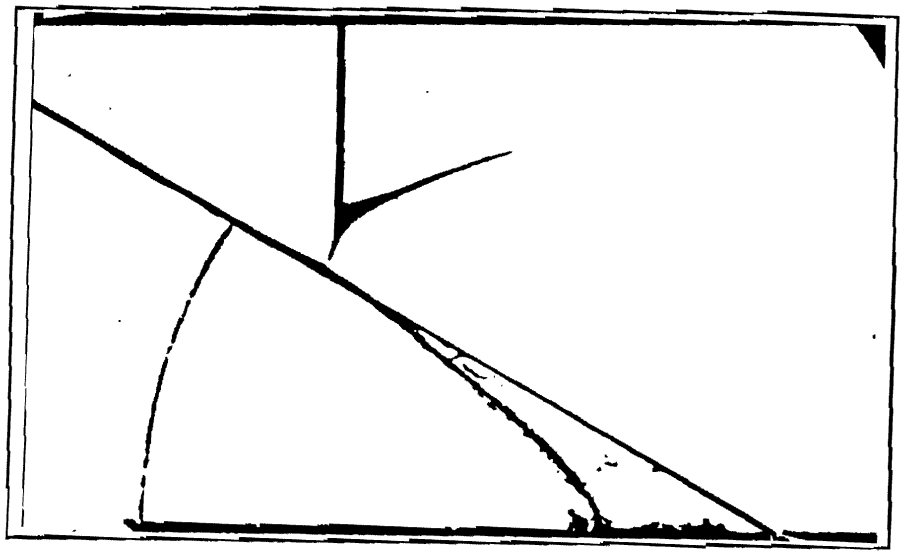

FIGURE 5. (a) Schlieren photograph and (b, c) colour contour plots for a weak irregular shock refraction, FNR at a CO_2/CH_4 gas interface with $\xi_i = 0.78$ and $\alpha_i = 60°$.

waves or weak contact discontinuities – than black and white, or shades or grey. For example, compare the clarity of the two contact discontinuities cd_1 and cd_2 (figures 2*f* and 10*e*) which emanate from the two shock triple points in figures 8(*e*) and 9(*b*). Or compare the detail with which the reflected shock *r* and expansion *e* are displayed in the schlieren photograph in figure 14(*a*) versus the colour contour plots in figure 14(*b*).

4.3. *Structure of the weak irregular refraction systems*

4.3.1. *The bound precursor refraction system, BPR*

The regular systems RRE and RRR are well described by the von Neumann theory, and in more detail by our numerical results. When the shock critical angle is exceeded, $\alpha_i > \alpha_{sc} \approx 34.4885°$, the RRR system becomes augmented with an expansion wave *e*, which appears in the receiving gas (CH_4), and with its pressure contours apparently centred on the refraction point *R* (figures 3*e*, 4*e*). The contours at first diverge as they move away from *R*, but then swing around and refract into the incident gas (CO_2) where they converge into a compression downstream of the reflected shock *r*. According to the von Neumann theory, there are no physically acceptable solutions for $\alpha_i > \alpha_{sc}$, and the impedances of the transmitted and reflected waves are unreal. For these reasons the system is irregular. The *r* and *t* shocks now have sharply increased curvatures near *R*, and furthermore *t* is now locally inclined forward of *R*, $\alpha_t > \frac{1}{2}\pi$ (figure 4*e*). By contrast, for the regular systems *t* is everywhere inclined backwards, $\alpha_t < \frac{1}{2}\pi$ (figure 4*a–d*). Thus *t* is a precursor wave for $\alpha_i > \alpha_{sc}$, and because it apparently moves along the gas interface at the same velocity as *i* and *r*, that is (1.9) remains satisfied, *t* is therefore also *a bound* precursor. Like Abd-El-Fattah & Henderson we shall call this system a 'bound precursor refraction' (BPR). In summary a BPR differs from an RRR both by the appearance of a fourth wave

(b)

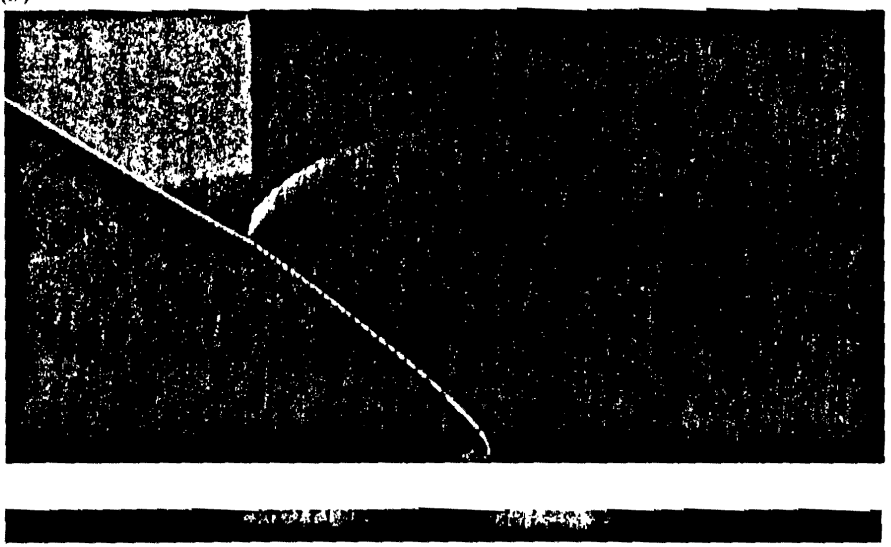

-0.328 0.231

(c)

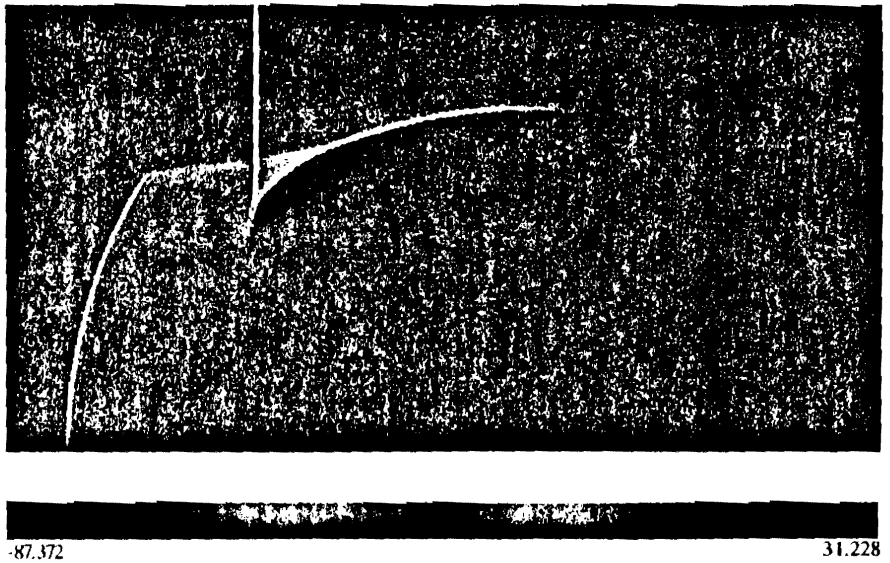

-87.372 31.228

FIGURE 5(*b,c*). For caption see facing page.

(b)

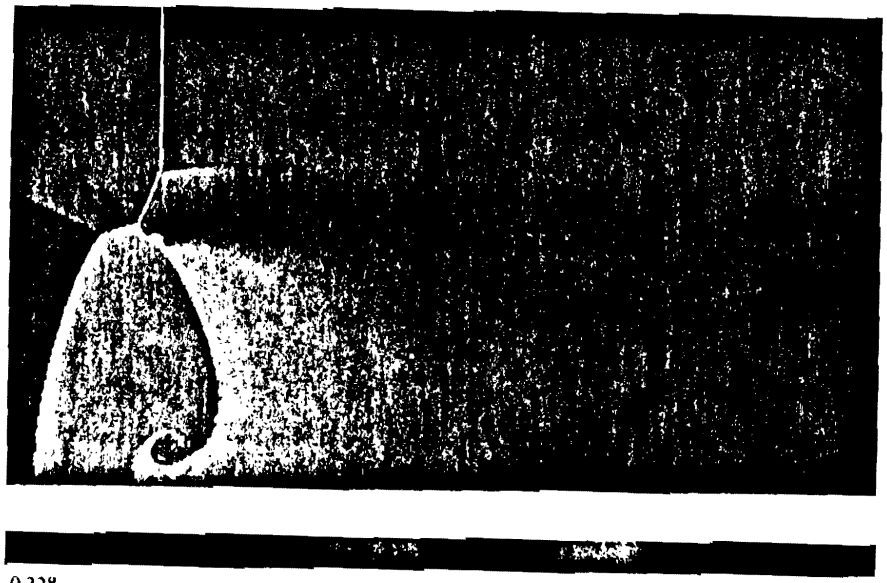

-0.328 0.765

(c)

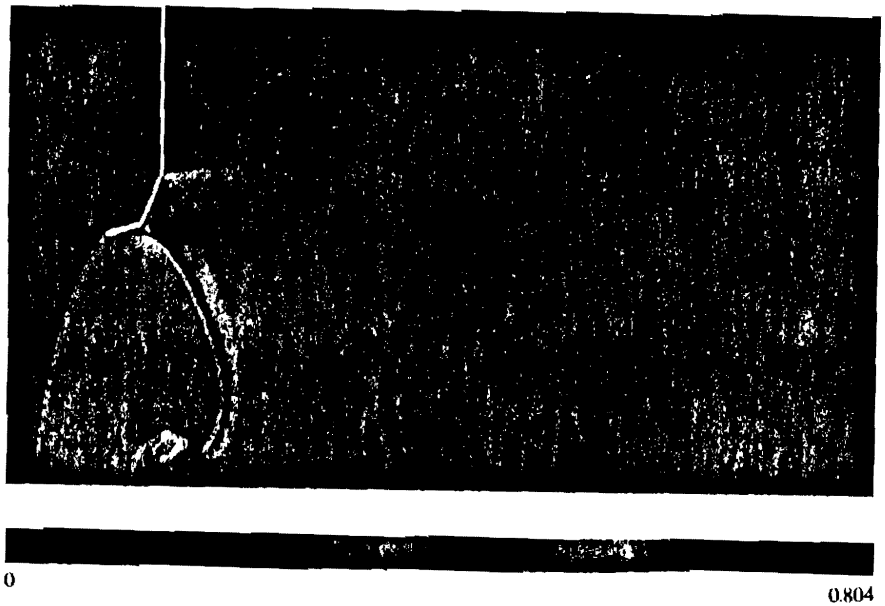

0 0.804

FIGURE 9(b,c). For caption see facing page.

(a)

FIGURE 9. (a) Schlieren photograph and (b,c) colour contour plots for a twin Mach reflection type refraction, TMR (see figure 2f), with $\xi_i = 0.18$ and $\alpha_i = 66°$ at a CO_2/CH_4 gas interface.

and by the fact that t leans forward ($\alpha_i > \frac{1}{2}\pi$) at the interface, whereas it leans backwards ($\alpha_i < \frac{1}{2}\pi$) for a RRR. The detailed structure of the BPR and especially of the fourth wave as displayed in figure 4(e) have not been reported previously to our knowledge. Indeed some doubt has been expressed as to whether a BPR is a basic system or is merely an experimental artifact (Catherasoo & Sturtevant 1983). Our numerical results provide good evidence to support the existence of it as a basic system.

4.3.2. *The condition for the RRR⇌BPR transition*

The shock critical angle α_{sc} is defined by the double root $\lambda_1 \equiv \lambda_2$ of the von Neumann theory (figure 3d), and this amounts to a generalization of the well-known shock detachment criterion for regular/irregular transition in shock *reflection*. Inspection of the polar diagrams reveals that the flow downstream of the reflected shock is always supersonic, $M_2 > 1$, for the λ_1 solution, and accordingly the sonic criterion (or its generalization to refraction) proposed by Hornung & Taylor (1982) cannot exist for the reflected shock. However, it *can* exist for the transmitted shock t, and in fact it does exist at an α_i about 1° smaller than α_{sc}. This difference is too small for experiment to discriminate, and we have not done the detailed and expensive computations necessary to decide the matter. Although the numerical data show that the RRR⇌BPR transition is close to the generalized detachment/sonic point for the t shock, experiment suggests that transition is delayed to values of α_i somewhat larger than $\alpha_i = \alpha_{sc}$. In the experiments transition is somewhat obscured by the wire frame on which the membrane was mounted, and also by a thin film of silicone oil which was used to seal the wire to the shock tube windows to reduce gas leakage. In view of this we conclude that transition occurs either at the generalized detachment/sonic point, or close to it.

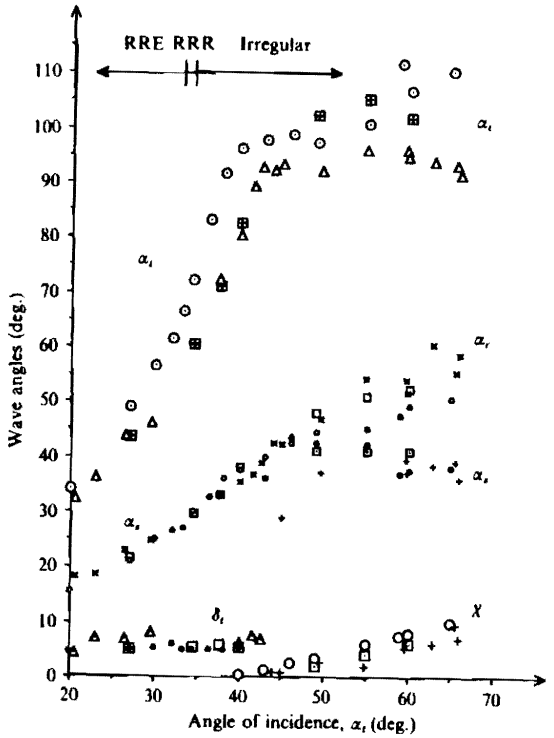

FIGURE 6. Experimental and computational wave angle data for a CO_2/CH_4 gas interface with $\xi_i = 0.78$. Square symbols represent data from computations with a 10% contamination of the CH_4 by the CO_2. Circular symbols represent data from computations with pure gases. All other symbols represent experimental data. ⊞, ⊙, △. Transmitted shock angle α_t: □, ○, ×, reflected wave angle α_s or α_r; □, ●, +, side shock angle α_s; □, ○, △, interface deflection angle δ_t; ⊡, ⊙, +, trajectory path angle χ; see figure 2 for the definition of the wave angles. (Experimental data from Abd-El-Fattah & Henderson 1978*b*.)

It is interesting to note that the condition $\alpha_t = \frac{1}{2}\pi$ must also be attained during the transition RRR $\rightleftharpoons$ BPR, because as this occurs we have seen that $(\alpha_t < \frac{1}{2}\pi) \rightarrow (\alpha_t > \frac{1}{2}\pi)$. Therefore the condition corresponding to the normal critical angle α_c defined by (1.12) is *forced* to occur at the same condition as the shock critical angle α_{sc}, even though $\alpha_{sc} < \alpha_c$.

4.3.3. *The free precursor refraction system, FPR*

With steadily increasing α_i, the t wave eventually breaks loose from the i and r shocks and runs ahead of them along the gas interface (figure 4*f*–*h*). The refraction law has now been violated as with expression (1.10), and there is now a *free* precursor refraction (FPR) in which the t wave moves ever further ahead of i and r with time.

It will be noticed that the pressure contours for the t wave are now spread out at, and near, the gas interface (figure 4*f*–*h*), instead of being concentrated as for a shock (figure 4*e*). Thus t is a locally smeared out or *evanescent* wave. However, further away from the interface the contours do converge to form a coherent shock. The t wave is itself refracted from the CH_4 back into the CO_2, which means that its refraction is

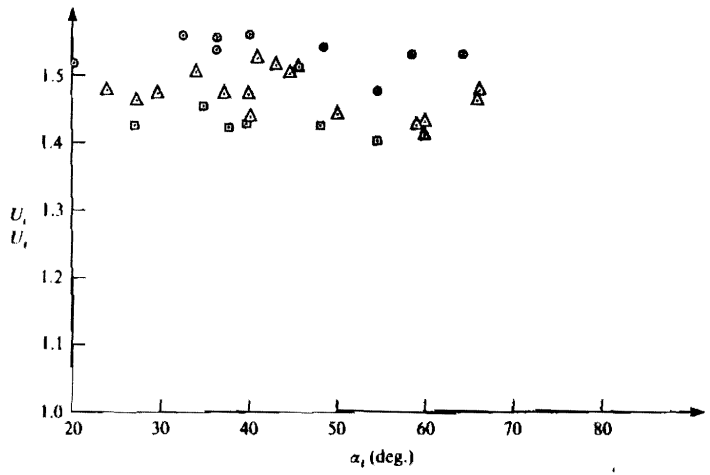

FIGURE 7. Comparison of the wave speed ratio U_i/U_t (see figure 2*c*) for a CO_2/CH_4 gas interface with $\xi_i = 0.78$. ⊙, Computed data for pure gases; ⊡, computed data for 10% contamination of the CH_4 by the CO_2; △, experimental data (from Abd-El-Fattah & Henderson 1978*b*).

locally fast–slow, $n > 1$. The wave transmitted into the CO_2 is the side wave s (figure 3*f*, *g*), and it is also an evanescent wave. Since locally $n > 1$, then $|\alpha_t| > |\alpha_s|$. The contour plots show no sign of a reflected wave from the t–s refraction, nor does there seem to be one in the experiments (presumably it is too weak to be resolved). Thus the local system appears to consist only of the t–s pair. The s wave and the incident shock i eventually encounter, and mutually modify, each other. The s contours converge to the reflected shock r after passing through i. The modified shock k, continues to the disturbed gas interface where it is locally refracted with total internal reflection $R = -1$, $T = 0$, $Z_t = 0$. This means that k is reflected as a centred expansion wave, e. This last wave eventually overtakes r and causes almost complete mutual cancellation, so that finally a weak reflection is propagated into the downstream CO_2 (figure 4*f*–*h*). It is clear from both the experimental and numerical results that s is an evanescent wave. The numerical results show that t is also evanescent but the experiments cannot resolve it. Hence the computation are predicting a new result for this wave.

It is natural to consider the conditions where a bound precursor system becomes a free precursor system or vice versa, BPR $\rightleftharpoons$ FPR. This is associated with the spreading out of the t wave into a distributed compression near the interface and it then runs ahead of the i and r shocks along the interface. Therefore the transition occurs with the violation of the refraction law (1.9), in other words (1.10) now applies. The law is of course immediately re-established for the precursors

$$\frac{|U_s|}{\sin\alpha_s} = \frac{|U_t|}{\sin\alpha_t}.$$

4.3.4. *The free precursor von Neumann refraction system, FNR*

Transition to yet another irregular refraction takes place as α_i continues to increase. It is characterized by a weak Mach reflection appearing in the CO_2. Some pressure contours of it are presented in figure 4(*h*) and a schlieren photograph and colour graphics in figure 5(*a*–*c*). Abd-El-Fattah & Henderson (1978*b*) called this a

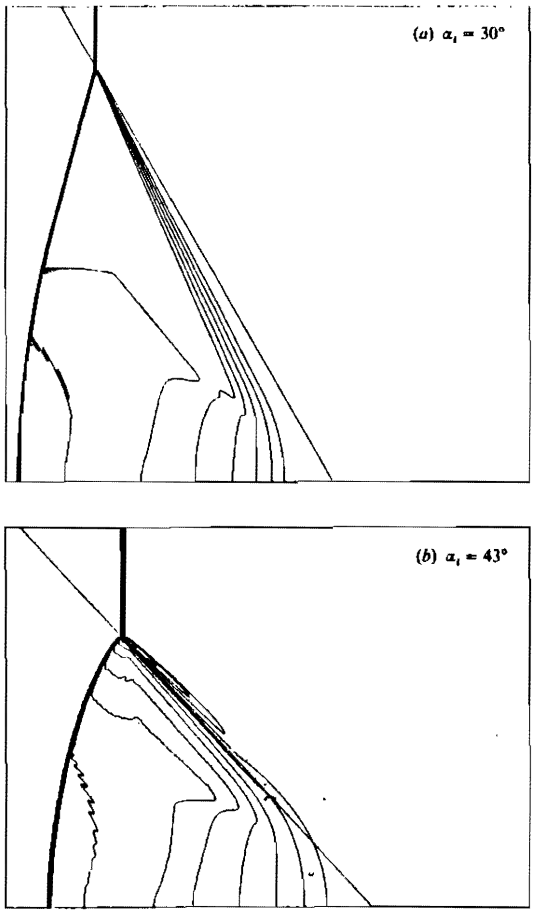

FIGURE 8(a, b). For caption see facing page.

'free precursor von Neumann refraction' (FNR). See figures 2(*d*), 3(*g*), 4(*h*), and 5(*a*–*c*) of this paper. The conditions for the FPR⇌FNR transition are not known and our computations are not sufficiently detailed to form a hypothesis with any confidence.

In summary the sequence of phenomena for the refraction of a weak shock at a slow–fast gas interface with increasing angle of incidence α_i is as follows:

$$\text{RRE} \rightleftharpoons \text{RRR} \rightleftharpoons \text{BPR} \rightleftharpoons \text{FPR} \rightleftharpoons \text{FNR}.$$

This sequence seems to be generally well supported by both the computations and by the experiments.

4.4. *Comparison of the numerical results with experiment*

In the interests of making the comparison as precise as possible we used the same values of the parameters $(\gamma_t, \gamma_i, \mu_t, \mu_i, \xi_t, \alpha_i)$ for our input data as Abd-El-Fattah & Henderson measured in their experiments. This included using the data for the

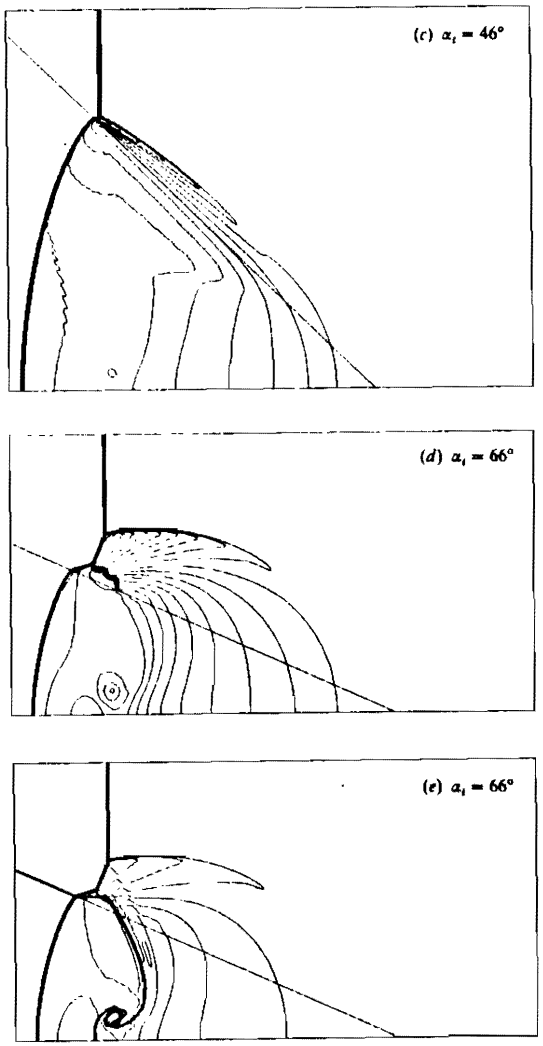

FIGURE 8. Contour plots of (*a*–*d*) log *P* and (*e*) log ρ from computations of a strong shock refraction sequence, $\xi_i = 0.18$, at a pure CO_2/CH_4 gas interface. (The straight line running diagonally from upper left to lower right represents the initial, undisturbed gas interface. It is not a pressure contour.)

contaminated gas shown in table 1, and the same boundary configuration. Some of the computations were repeated for the pure gases in order to obtain an estimate of the sensitivity of the results to gas contamination. The numerical data for the pure and the contaminated gases are compared with experiment in figures 6 and 7. Figure 6 shows a variety of wave angles as well as the interface deflection angle δ_i (figure 2*a*) and the trajectory path angle χ for the intersection of the i, k, s and s' waves (figure 2*d*). For the regular part of the sequence, RRE⇌RRR, the numerical results for the

contaminated gas are everywhere in satisfactory agreement with experiment, but the corresponding results for the pure gases show a significant discrepancy for the α_t data, but not for the α_r, α_e, and δ_t data. So only the α_t data seem to be sensitive to contamination, and that sensitivity is greatest near transition $\alpha_t = \alpha_{sc} \approx 34.4885°$ ($\lambda_1 \equiv \lambda_2$) where small variations in the contamination can cause significant changes to α_t. Thus, for regular refraction the α_t data are sensitive to contamination while the data for other angles are not. This is ascribed to the fact that incident and reflected waves propagate in the CO_2 which is little affected by contamination because of the large fraction of the volume it occupies in the shock tube, while the t wave propagates in the CH_4 and this *is* significantly affected (table 1).

After transition to irregular refraction the numerical data for the contaminated gas are again in agreement with experiment so long as, approximately, $\alpha_t < 50°$; but significant discrepancies are evident for $\alpha_t > 50°$, particularly for the α_t data. For irregular refraction the t wave is everywhere curved, and as $\alpha_t > 50°$ increased we found that this curvature became quite sharp near the gas interface. This made the choice of where to draw the tangent to t in order to measure α_t at the interface increasingly uncertain. The same difficulty occurred for both the schlieren photographs and for the contour plots. We therefore looked for more robust data to compare with the experiment, which we found in the measurements of the wave velocities U_t and U_t. The numerical data for U_t/U_t are compared with experiment in figure 7. These data include the computations for the pure and the contaminated gases, and it will be noted that the results bracket the experiment data.

It should be remarked that the measurements of the gas contamination are only average values obtained after the contaminated gases had been drawn from the shock tube and individually sent to the thermal conductivity meter. Therefore the local contamination near the gas interface could have been significantly different from the average value obtained at the meter. In view of the uncertainties involved we conclude that the agreement between the numerical data and experiment is satisfactory.

5. Results and discussion for a strong refraction sequence

5.1. *Wave structures in the sequence*

A second series of computations was done for the CO_2/CH_4 interface, except that i was now a strong shock, $\xi_i = 0.18$; this work was restricted to the pure gases. Selected contours are presented in figure 8, and a schlieren photograph together with colour graphics are presented in figure 9 (plate 2). A comparison with experiment cannot be precise because the effect of gas contamination has not been taken into account in the computations. However, note that the computational results in figures 9(*b*) and 9(*c*) clearly display all of the key features of the refraction found in the schlieren photo in figure 9(*a*), especially the two-shock triple points i-n-r and s-n-r' and the two contact discontinuities cd_1 and cd_2 emanating from these triple points (figure 2*f*).

The polar diagrams are presented in figure 10. When α_t is small enough to result in regular refraction, the von Neumann theory provides three physically acceptable solutions, namely two with reflected shocks λ_1, λ_2 and one with a reflected expansion ϵ_1 (figure 10*a*). It was the ϵ_1 (RRE) solution which Abd-El-Fattah & Henderson observed. With increasing α_t one obtains the coincidence $\lambda_1 \equiv \lambda_2 \equiv i \equiv A_1$, and then the reflected shocks in the λ_1, λ_2 (RRR) solutions degenerate to Mach lines (figure 10*b*).

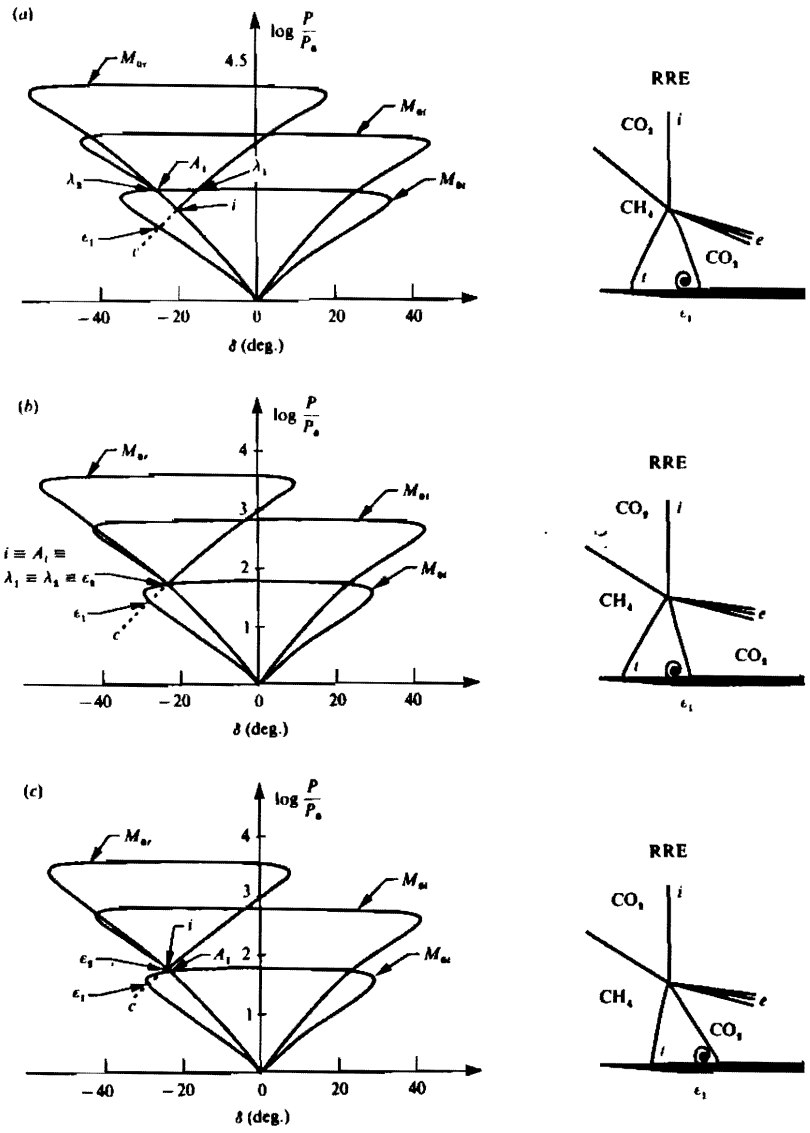

FIGURE 10(*a–c*). For caption see next page.

Although this takes place at the angle of intromission $\alpha_{tm} \approx 35.94°$, it has no physical significance in this case because ϵ_1 is not degenerate at this condition. Hence the impedances are *not* equal, $Z_t \neq Z_t$, for the solution ϵ_1 that is actually observed.

For $\alpha_t > \alpha_{tm}$, the λ_1, λ_2, solutions are unreal and at the same time we obtain a second solution ϵ_2 of the RRE type (figure 10*c*). However, once more it was the ϵ_1 solution that Abd-El-Fattah & Henderson observed. Clearly, at $\alpha_t = \alpha_{tm}$ the coincidence can be extended to ϵ_2; thus, $\lambda_1 \equiv \lambda_2 \equiv \epsilon_2 \equiv i \equiv A_1$. Notice, however, that

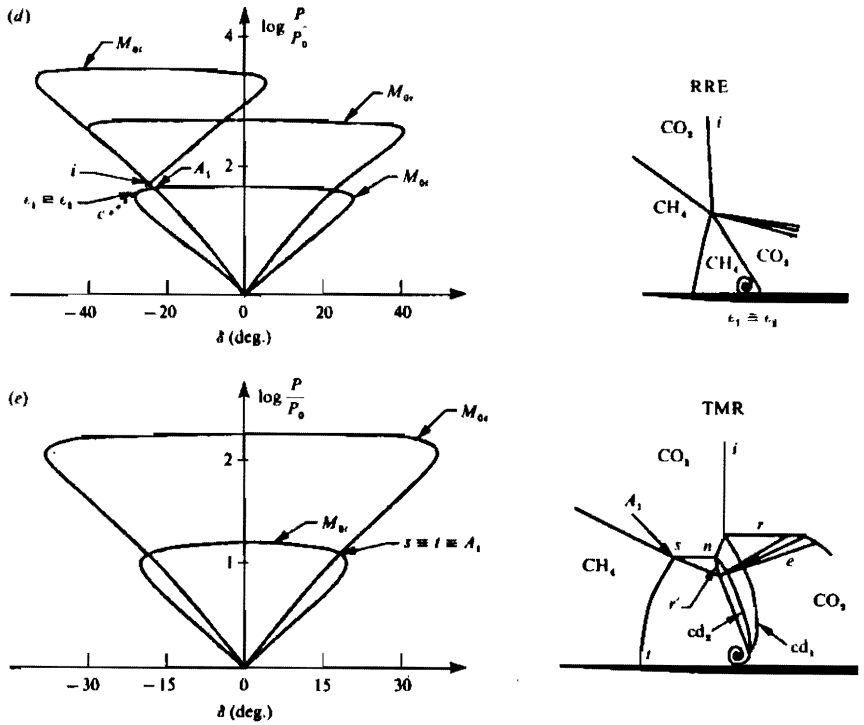

FIGURE 10. Polar diagrams for a strong shock refraction sequence with $\xi_i = 0.18$ at a pure CO_2/CH_4 gas interface. (*a*) RRE, ϵ_1 solution at $\alpha_i = 30°$; (*b*) RRE, ϵ_1 solution at $\alpha_i = \alpha_{sc} = 35.95°$. Note that ϵ_1 is not a continuation of either the λ_1, or λ_2 solutions, therefore the shock critical angle for $\lambda_1 \equiv \lambda_2$ is irrelevant for transition to irregular refraction in this case; (*c*) RRE, at $\alpha_i = 37°$; note there are now two RRE solutions, ϵ_1 and ϵ_2; the ϵ_1 solution is observed in experiments; (*d*) RRE, at the relevant shock critical angle, $\epsilon_1 \equiv \epsilon_2$, $\alpha_i = \alpha_{sc} = 46.294°$; this is the transition condition for RRE$\rightleftharpoons$TMR; (*e*) twin Mach reflection–refraction TMR at $\alpha_i = 66° > \alpha_{sc}$.

the ϵ_1 solution nowhere forms a coincidence with either the λ_1, λ_2 solutions as it did at the A_1 point in the weak sequence. Consequently, by continuity no refraction of the RRR type can appear in this strong sequence.

As α_i continues to increase one eventually obtains $\epsilon_1 \equiv \epsilon_2$ (figure 10*d*), where the isentropic c is tangent to the t polar. This again occurs at the shock critical angle $\alpha_{sc} \approx 37.79°$, but it differs from the weak series in that the coincidence is an RRE type $\epsilon_1 \equiv \epsilon_2$, instead of the RRR type, $\lambda_1 \equiv \lambda_2$.

For $\alpha_i > \alpha_{sc}$, the refraction is irregular and both the experiments and the computations agree that it is again a free precursor system. However, the numerical results show that both the t and the s waves are shocks and not evanescent compressions as they were in the weak sequence. Structurally the system consists of the precursor transmitted-side shock pair t-s, interacting with a single Mach reflection triplet of shocks i–r–n (figure 10*e*). The side shock s now interacts with the *Mach* shock n, modifies it and produces the second reflected shock r'. Consequently, there are two Mach reflections in the incident gas, i–n–r, and s–n–r', the refraction will be called a '*twin Mach reflection–refraction*' (TMR). The r' shock undergoes total internal reflection at the disturbed gas interface and gives rise to the reflected

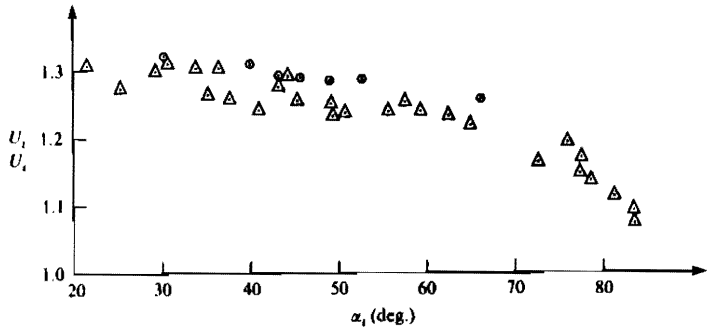

FIGURE 11. Comparison of the wave speed ratio U_t/U_i (see figure 2*c*) for a CO_2/CH_4 gas interface with $\xi_i = 0.18$. ⊙, Computed data for pure gases; △, experimental data (from Abd-El-Fattah & Henderson 1978*b*).

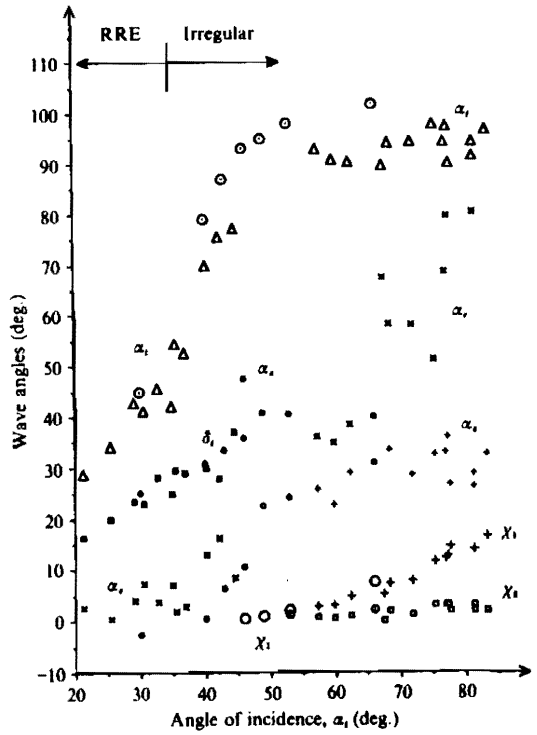

FIGURE 12. Experimental and computational wave angle data for a CO_2/CH_4 refraction with $\xi_i = 0.18$. Circular symbols represent data from computations with pure gases. All other symbols represent experimental data. ⊙, △, Transmitted shock angle α_t; ○, ×, reflected wave angle α_r or $\alpha_{r'}$; ●, +, side shock angle α_s; ○, ⊡, interface deflection angle δ_i; ○, +, trajectory path angle χ_1; ⊙, □, trajectory path angle χ_2. (Experimental data from Abd-El-Fattah & Henderson 1978*b*.)

(a)

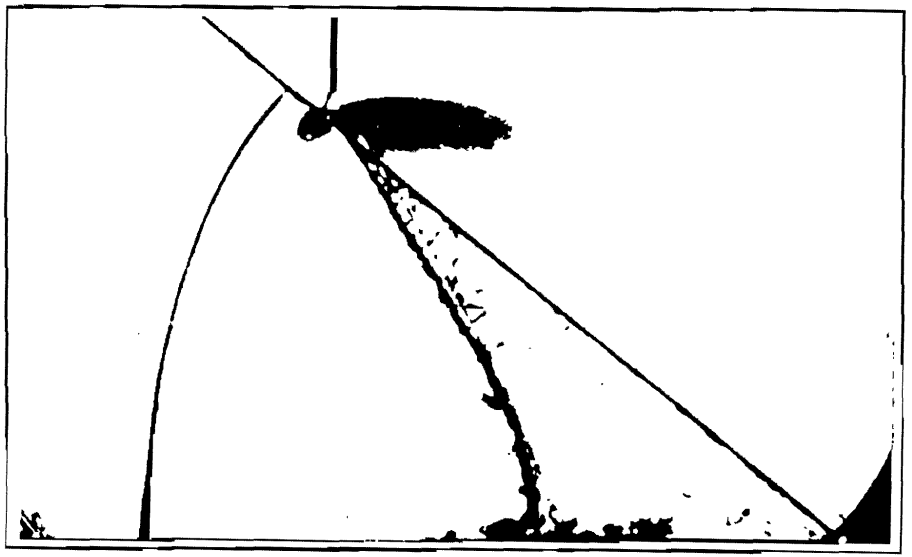

FIGURE 13. (a) Schlieren photograph and (b, c) colour contour plots for a twin regular reflection type refraction, TRR (see figure 2e) $\xi_i = 0.53$, $\alpha_i = 50.5°$, at a CO_2/CH_4 gas interface. See also the caption to figure 5.

expansion e, which in turn overtakes and attenuates r. Contact discontinuities cd_1 and cd_2 appear at the MR triple points (figures 2f, 8e, 9a, b and 10e); of course they are not visible in figures 8(d) and 9(c) since these are contours of log p. There are now three shear layers in the downstream flow, namely cd_1 and cd_2, and the disturbed gas interface.

5.2. *Comparison of the numerical results with experiment*

The numerical results are compared with the experiments data in figures 11 and 12. As expected the discrepancy for the α_t data is comparatively large because we did not take into account the gas contamination. Qualitatively it is similar to the discrepancy for the weak series in figure 6. The increasing size of the discrepancy for the irregular refraction is again attributed to the uncertainty of measuring α_t with increasing curvature of the t shock near the interface. The angle data for χ_1, χ_2, and δ_t, are generally in satisfactory agreement, granted the numerical and experimental uncertainties. These last measurements were made either for the CO_2 flow field, or along its boundary (δ_t) and, as we have seen, such measurements are insensitive to gas contamination. The curvature of the reflected shock r prevented us from making reliable measurements of α_r, while the short length of the side shock s similarly prevented reliable measurements of α_s. The discrepancies for α_r and α_s are significant and are attributed to these uncertainties.

In figure 11 the numerical data for U_t/U_i display a small systematic discrepancy from the experimental data. This is qualitatively similar to the pure gas results shown in figure 7, and is ascribed to the same cause, namely gas contamination. Nevertheless, the agreement with experiment is quite reasonable.

(b)

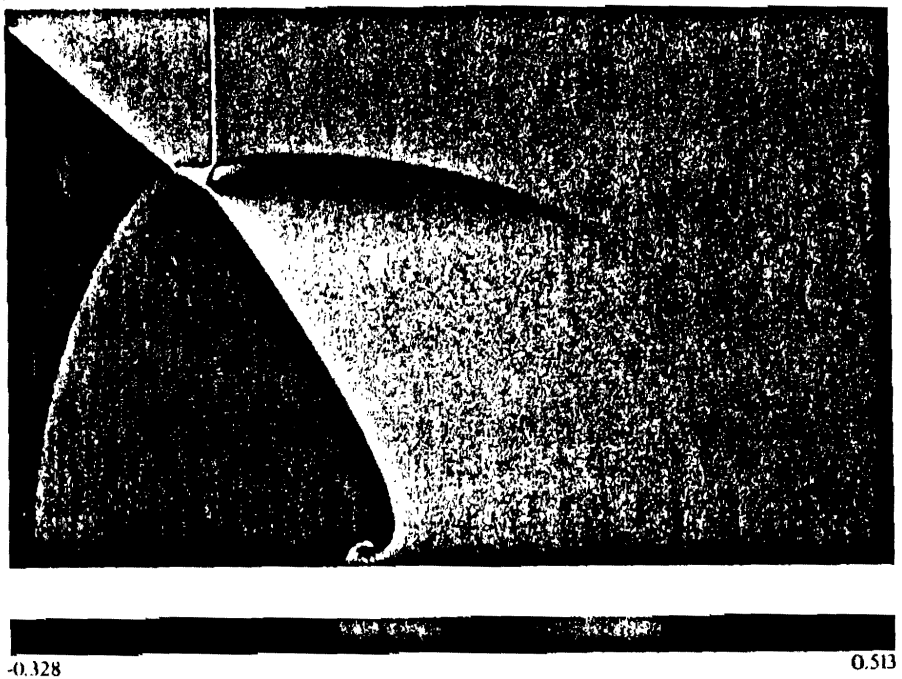

-0.328 0.513

(c)

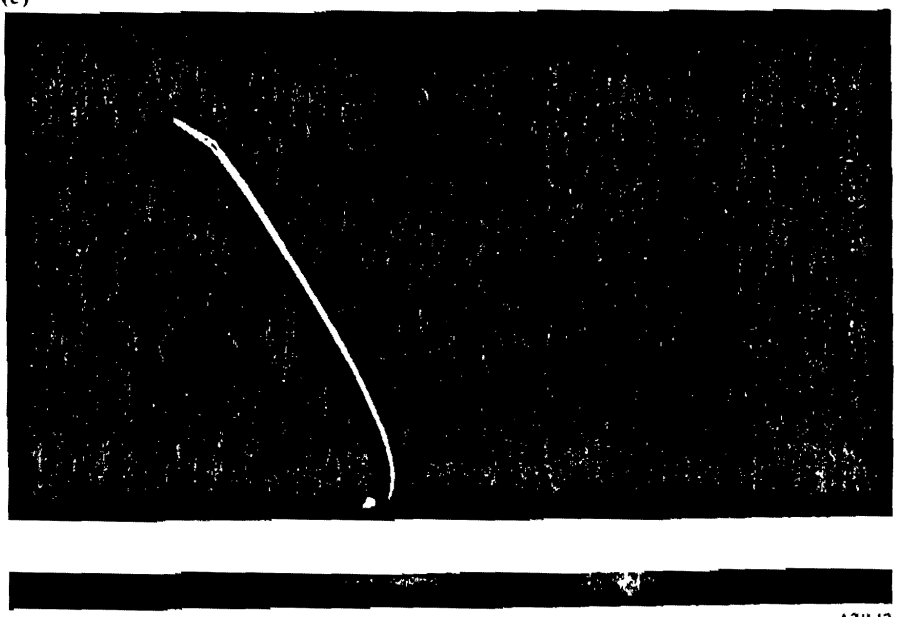

-28.308 138.13

FIGURE 13(b,c). For caption see facing page.

(b)

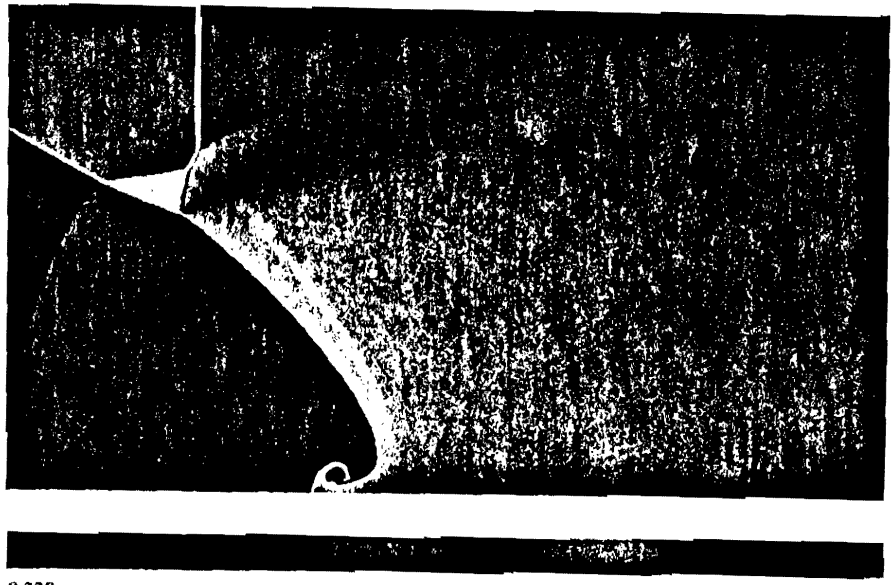

-0.328 0.450

(c)

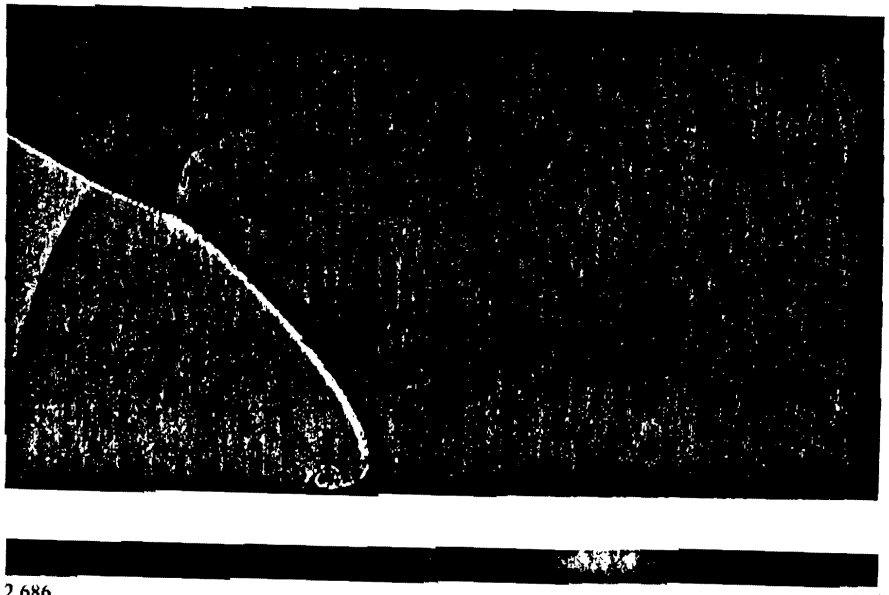

2.686 8.386

FIGURE 14(b,c). For caption see facing page.

(a)

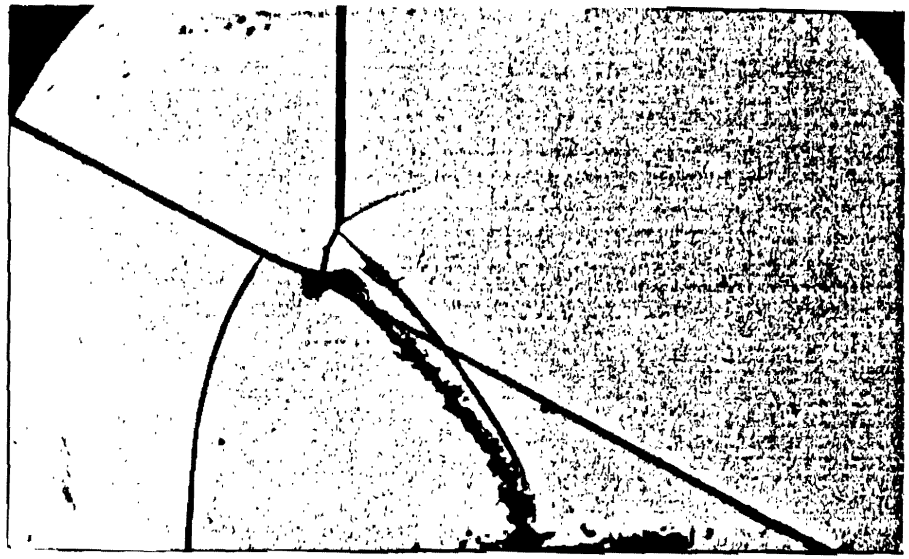

FIGURE 14. (a) Schlieren photograph and (b,c) colour contour plots for a twin von Neumann irregular refraction, TNR (Abd-El-Fattah & Henderson 1978b) at a CO_2/CH_4 gas interface with $\xi_i = 0.53$ and $\alpha_i = 62°$.

6. The boundary between the strong and the weak systems

We consider how a weak irregular refraction may be changed into a strong one, or vice versa, FNR $\rightleftharpoons$ TMR. This will be done by continuously reducing ξ_i from $\xi_i = 0.78$ where the system is weak, to $\xi_i = 0.18$, where it is strong. In the following discussion the parameters $(\gamma_t, \gamma_i, \mu_t, \mu_i)$ will be held constant and α_i will be allowed to vary only slightly while ξ_i is decreased. We begin by considering the weak, irregular refraction that we call FNR at $\xi_i = 0.78$ (figures 4*h* and 5*a–c*). As ξ_i decreases the shock triple points F_1, F_2 (figures 2*f* and 3*g*) continuously approach the quadruple point G (figure 2*e*) and then for some ξ_i they coincide with it, $F_1 \equiv F_2 \equiv G$. The weak Mach reflection has now vanished and the number of shocks in the incident gas are reduced to four, *i–s–r–k* (figure 2*e*). If we imagine that the CH_4 is replaced by a rigid medium with the same boundaries, then the four-shock interaction would amount to the twin regular reflection studied by Smith (1959). Since the *i* and *s* shocks are generally of unequal strength, their interaction is asymmetrical and a contact discontinuity arises in the downstream flow. A schlieren photograph of this refraction, obtained by Abd-El-Fattah & Henderson with $\xi_i = 0.53$ and $\alpha_i = 50.5°$ is presented in figure 13(*a*), together with colour contour plots from the computations in figure (13*b*, *c*) (plate 3). We shall call it a twin regular reflection–refraction (TRR). Actually the cited authors found that this system existed for a range of ξ_i and not just for a particular value on the boundary between the strong and the weak systems. If $\xi_i = 0.53$ is held constant and α_i is now increased to $\alpha_i = 62°$, then the four-shock system changes into the twin von Neumann system (TNR) (Abd-El-Fattah & Henderson 1978*b*) shown in figure 14 (plate 4). Eventually, however, as ξ_i becomes small enough the four-shock system in the TRR changes to the twin Mach reflection characteristics of a TMR at $\xi_i = 0.18$, and $\alpha_i = 66°$ (figures

2*f*, 8*d*, *e*, 9, and 10*e*). The condition for the TRR⇌TMR transition have been discussed by Smith for reflection, and Abd-El-Fattah & Henderson for refraction.

A variety of special conditions may be used to define precisely the strong/weak boundary. Some of them have been discussed by the above authors. Here we notice that for weak systems the regular/irregular transition RRR⇌BPR takes place at the von Neumann tangency point $\lambda_1 \equiv \lambda_2$, that is at α_{sc}, but for strong systems the tangency condition has a different character $\epsilon_1 \equiv \epsilon_2$, so RRE⇌TMR, but again at α_{sc}. It seems plausible therefore to define the strong/weak boundary at the point where *both* conditions are in coincidence, $\lambda_1 \equiv \lambda_2 \equiv \epsilon_1 \equiv \epsilon_2 \equiv i \equiv A_1$. For the pure gas interface CO_2/CH_4 this is approximately at $\xi_b \equiv \xi_t = 0.471$ and $\alpha_t = 34.05°$. So an incident shock i has a weak refraction whenever $\xi_t > \xi_b$ and a strong one when $\xi_t < \chi_b$.

Abd-El-Fattah & Henderson used a different condition for the boundary, based upon a generalization of the von Neumann classification for shock reflection, but the definition of the boundary is somewhat arbitrary.

There is some hint that in our results for the strong sequence $\xi = 0.18$, the four-shock TRR system appears immediately after transition to an irregular refraction. However, it is not resolved unequivocally, and in any event a TMR is certainly present when α_t increases by only a small further amount.

Each regular or irregular wave system occurs for definite ranges of values of the system parameters $(\gamma_i, \gamma_t, \mu_i, \mu_t, \xi_t, \alpha_t)$, and it is possible to produce a topological plot of ξ_t versus α_t for a given combination of gases $(\gamma_i, \gamma_t, \mu_i, \mu_t)$. Abd-El-Fattah & Henderson (1978*b*) did this for the CO_2/CH_4 interface and we refer the interested reader there for further details.

7. Concluding remarks

In our computations of the weak refraction sequence we used the same input data as Abd-El-Fattah & Henderson had measured in their experiments. This included the effects of gas contamination due to leakage and diffusion across the membrane, and also the inertia of the membrane. The object was to test the validity of the computations by obtaining as precise a comparison with experiment as possible. We found that the membrane inertia made very little difference and we ignored it in our later computations. However, our data for the wave angle α_t of the transmitted shock was sensitive to gas contamination, and to a lesser extent so was the wave velocity U_t data of this shock. None of the other data displayed such sensitivity, and this was ascribed to the fact that α_t and U_t were measured for the CH_4 component which was significantly affected by contamination (table 1) whereas the other data, χ, α_r, α_s, and so on, were measured for the CO_2 component which was very little affected by the contamination.

Our computations were everywhere in reasonable agreement with experiment when gas contamination was taken into account, except for the α_t data when, approximately, $\alpha_t > 50°$. That discrepancy was ascribed to the uncertainty of making accurate measurements of α_t owing to the increasingly large curvature of the transmitted wave with increasing α_t. This uncertainty applied to both the experimental data and to measurements made from the contour plots.

The computations were done for inviscid gases and since the results were generally in good agreement with experiment it is concluded that viscosity had no significant effect on the measurements. Presumably viscosity would be of most importance in

gases. The computations allowed vorticity production and transport but not viscous diffusion.

The computations resolved the structure of the bound precursor refraction (BPR), and revealed the presence of a fourth wave, which was an expansion and apparently centred on the refraction point. After transition to a free precursor system, BPR⇌FPR, the transmitted/side shock pair were found to be smeared out in the region of the gas interface, which we called evanescent waves.

Similar effects were found in our computations for stronger refraction and were ascribed to the same causes. Our computations displayed all the principle features found in experiment, such as local single Mach reflection–refractions, twin Mach reflection refractions, free precursor shocks, contact discontinuities, reflected expansion waves, and so on. In particular our computations were able to accurately and sharply resolve contact discontinuities, for example those emanating from shock triple points (figures 10, 13, and 14). This has historically been a difficult task for numerical methods primarily designed to capture shocks. We conclude that the code does provide a satisfactory representation of the refraction phenomena even though it ignores the effects of viscosity and three-dimensionality.

This work was performed under the auspices of the US Department of Energy at the Lawrence Livermore National Laboratory under contract number W-7405-ENG-48 and partially supported by the Applied Mathematical Sciences subprogram of the Office of Energy Research under contract number W-7405-Eng-48 and the Defense Nuclear Agency under IACRO 88-873.

REFERENCES

Abd-El-Fattah, A. M. & Henderson, L. F. 1978*a* *J. Fluid Mech.* **86**, 15.

Abd-El-Fattah, A. M. & Henderson, L. F. 1978*b* *J. Fluid Mech.* **89**, 79.

Abd-El-Fattah, A. M., Henderson, L. F. & Lozzi, A. 1976 *J. Fluid Mech.* **76**, 157.

Berger, M. J. & Colella, P. 1989 *J. Comput. Phys.* **82**, 64.

Bitondo, D. 1950 *Inst. Aerophys., University of Toronto, UTIA Rep.* 7.

Catherasoo, C. J. & Sturtevant, B. 1983 *J. Fluid Mech.* **127**, 539.

Colella, P., Ferguson, R. & Glaz, H. M. 1990 Multifluid algorithms for Eulerian finite difference methods. Preprint in preparation.

Colella, P. & Glaz, H. M. 1985 *J. Comput. Phys.* **59**, 264.

Colella, P. & Woodward, P. 1984 *J. Comput. Phys.* **54**, 174.

Glaz, H. M., Colella, P., Glass, I. I. & Deschambault, R. L. 1985 *Proc. R. Soc. Lond.* A **398**, 117.

Haas, J. F. & Sturtevant, B. 1987 *J. Fluid Mech.* **181**, 41.

Henderson, L. F. 1989 *J. Fluid Mech.* **198**, 365.

Hornung, H. G. & Taylor, J. R. 1982 *J. Fluid Mech.* **123**, 143.

Jahn, R. G. 1956 *J. Fluid Mech.* **1**, 457.

Leer, R. G. van 1979 *J. Comput. Phys.* **32**, 101.

Neumann, J. von 1943 In *Collected Works*, vol. 6, p. 1963. Pergamon.

Noh, W. F. & Woodward, P. 1976 *UCRL Preprint* No. 77651.

Schwendeman, D. W. 1988 *J. Fluid Mech.* **188**, 383.

Smith, W. R. 1959 *Phys. Fluids* **2**, 533.

Whitham, G. B. 1958 *J. Fluid Mech.* **4**, 337.

Whitham, G. B. 1959 *J. Fluid Mech.* **5**, 369.